Scientific Research Publishing

Open Journal of Applied Sciences, 2024, 14, 3261-3281
https://www.scirp.org/journal/ojapps
ISSN Online: 2165-3925
ISSN Print: 2165-3917

Study on the Effect of Magnetic Pole Clipping Angle on the Eddy Current Loss of Permanent Magnets in the Rotor of Magnetically Levitated Permanent Magnet Synchronous High-Speed Electric Spindles

Xiangjun Shen, Houcai Liu, Huimin Kang, Ruirong He, Jiale Xi

School of Mechanical and Electrical Engineering, Hunan University of Science and Technology, Xiangtan, China
Email: sxj928969286@163.com

How to cite this paper: Shen, X.J., Liu, H.C., Kang, H.M., He, R.R. and Xi, J.L. (2024) Study on the Effect of Magnetic Pole Clipping Angle on the Eddy Current Loss of Permanent Magnets in the Rotor of Magnetically Levitated Permanent Magnet Synchronous High-Speed Electric Spindles. *Open Journal of Applied Sciences*, **14**, 3261-3281.
https://doi.org/10.4236/ojapps.2024.1411216

Received: October 15, 2024
Accepted: November 25, 2024
Published: November 28, 2024

Abstract

Aiming at the problem of high temperature and even demagnetization failure of permanent magnet (PM) due to PM eddy current loss in PM synchronous high-speed motors, this paper proposes a technique to lessen PM eddy current loss by cutting the angle of PM poles to change the shape of PM structure. Firstly, an analysis is conducted on the mechanism of PM synchronous high-speed motor eddy current loss production, the theoretical analytical model of PM eddy current loss is deduced, and it is theoretically proved that the magnetic pole shaving angle can reduce PM eddy current loss. Then, a 25 KW surface-type PM synchronous high-speed motor as an object, using two-dimensional time-step finite element method (FEM) to model and analyze PM eddy current loss. The results show that the smaller the PM pole shaving angle, the less its eddy current loss will be, it is possible to minimize the pole shaving angle of eddy current loss by 9.8% compared to the unshaved angle. Finally, the temperature field of the PM is calculated using a finite element method, and the outcomes demonstrate that the maximum temperature of the PM with a magnetic pole shaving angle can be reduced by about 5% compared with the unshaved angle.

Keywords

Magnetic Pole Clipping, Permanent Magnet (PM), Eddy Current Loss,

Temperature Field, Two-Dimensional Time-Stepped Finite Element Method (FEM)

1. Introduction

Magnetic levitation permanent magnet (PM) synchronous high-speed electric spindle with high transmission efficiency, high rotary accuracy, frictionless, long service life, and can be actively controlled, extensively utilized in high-speed and ultra-high-speed machining machines [1]-[3]. Its built-in surface type PM synchronous motor rotor magnetic field in the process of coupling with the stator excitation magnetic field will result from the permeability harmonics' source of stator core slotting, stator winding uneven distribution of space harmonics, as well as stator excitation current due to the grid voltage fluctuations or the controller sideband impact of time harmonics generated by the stator excitation current [4], these harmonics will be high-speed cutting the rotor PM and the formation of closed loop, it ultimately results in the creation of eddy current losses and the emission of energy as heat. Because of the tiny size of the built-in PM synchronous spindle motor, the heat dissipation conditions are poor, the heat generated by eddy current loss will lead to high temperature of PM, and in serious cases, even result in demagnetization failure of PM, which greatly affects the reliability and stability of the spindle operation [5]. In order to improve the dependable and stable operation of magnetically levitated PM synchronous high-speed motor spindles, it is crucial to examine the mechanism of eddy current loss generation in PM synchronous motors, research the methodology for precisely calculating the eddy current loss of PM, and investigate structural optimization schemes to lower the eddy current loss of PM.

At present, domestic and foreign research around the PM synchronous motor eddy current loss calculation method is mainly reflected in the analytical method and finite element method (FEM). As in Literature [6], ignoring the effects of core saturation, magnetic leakage, and material nonlinearity and only considering the space harmonics caused by eddy current effect, magnetic conductivity harmonics caused by stator slotting and uneven eddy current distribution, the eddy current loss calculation model of the PM is deduced by the analytical method, and the eddy current loss data are obtained by the calculation of harmonic analysis method, and the information gathered from the experiments confirms that the computation is accurate. The two-dimensional time-stepped finite element method used in Literature [7] can not only take into account the eddy current effect and the cogging effect, but also the effects of core saturation, leakage, and nonlinear problems of the permeable materials on the magnetic field of the motor, and a more accurate result can be obtained in calculating the eddy current loss of the rotor of a high-speed PM motor. Literature [8] used the harmonic analysis method and time-step finite element method to calculate the harmonic loss of the motor rotor respectively, and

compared and analyzed with the experimental data, and the results show that the time-step finite element calculation results are more accurate. Although the analytical method can intuitively and quickly reveal the nature and law of the rotor eddy current loss, it can only be applied to a relatively special boundary situation, and it is difficult to take into account all the factors, while the FEM can be calculated regardless of the complexity of the boundary conditions and basically can take into account all the influencing factors.

Based on harmonic calculations, another part of scholars has conducted in-depth research on the methods of harmonic suppression. For example, Literature [9]-[11] cuts off the eddy current circuit of the PM by segmenting the PM of a non-high-speed PM motor, which significantly reduces the eddy current loss of the PM. However, Literature [12] suggests that for high-speed PM motors, the number of chunks should reach a certain number to effectively reduce the eddy current loss, and if the number of chunks is too small, it will increase the eddy current loss. Although the process difficulty of PM chunking is not large, the number of chunks is too large and impractical, so for high-speed motors, the method of chunking PM to suppress eddy current loss is not suitable at present. In Literature [13], harmonic magnetic field is suppressed by the method of unequal turns winding, and in Literature [14], the method of setting magnetic bridge in the stator yoke can also suppress harmonic magnetic field. Both methods can reduce the eddy current loss of permanent magnets. Literature [15] allows the shielding ring eddy current to eliminate part of the air gap harmonic magnetic field by adding a shielding ring of appropriate thickness inside the rotor sheath, thus improving the magnetic field waveform in PM and reducing the PM eddy current loss. Although the above methods can reduce eddy current losses, they all increase the difficulty of the motor manufacturing process.

Considering that the core of suppressing eddy current loss is to eliminate harmonic magnetic field effectively, and by optimizing the PM structure of the existing surface-type and tile-shaped PM synchronous motors, it can not only satisfy this requirement, but also has the advantages of simple structure, lower manufacturing cost, and easy to implement. Thus, based on the harmonic suppression idea of effectively eliminating part of the harmonic magnetic field and improving the air gap density waveform, this paper proposes a harmonic suppression method of chipping the PM structure of surface-type and tile-type PM synchronous motors by taking into account that chipping can reduce the equivalent air gap length, which is capable of reducing the flux rate of change, to reduce the magnetic flux density on the PM to reduce the eddy current loss. Based on the mechanical and electromagnetic parameters of a 25 KW surface-type PM synchronous motor, firstly, the effect of different clipping angles on the eddy current loss of a 4 mm-thick tile-type PM is calculated and analyzed using a two-dimensional time-stepping FEM. Then, the effect of different tile thicknesses on eddy current loss before and after PM chipping is investigated. Finally, the results of 2D time-step FEM are substituted into Ansys Icepak for thermal simulation to derive the temperature distribution of

the surface-type and tile-shaped PM synchronous motor spindles.

2. Analytical Computational Modeling of Eddy Current Losses in Permanent Magnets

2.1. Mechanism of Eddy Current Loss Generation in Permanent Magnets

Considering that the structure of permanent magnet synchronous motorized spindle is optimized in this paper, and the structural characteristics do not produce time harmonics, so only the eddy current loss caused by permeability harmonics and space harmonics is considered.

2.1.1. Generation of Magnetically Induced Harmonics

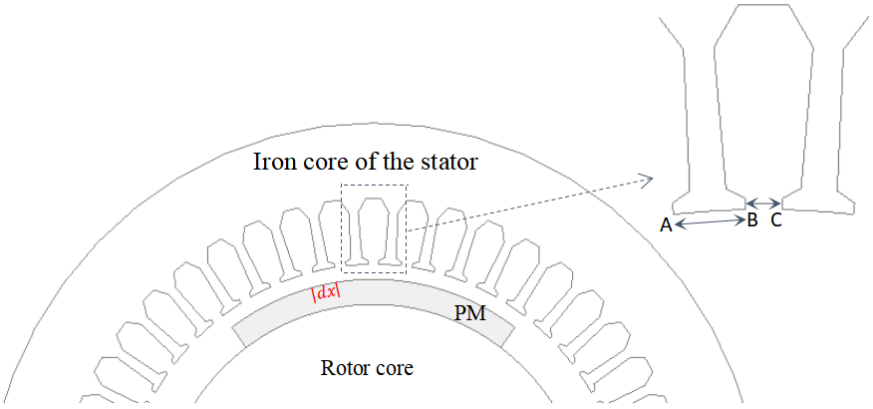

Figure 1. Schematic diagram of magnetic permeability change.

As shown in **Figure 1**, the permeability harmonics arise because the stator core is slotted, resulting in different permeabilities between the yoke and the gap. As the rotor rotates, the air gap permeability corresponding to any segment of arc dx on the permanent magnet is constantly changing. The air gap is small and the magnetic permeability is large when it is at AB under the teeth. While at slot BC, the air gap is larger and the permeability is small. This variation is periodic in terms of slot spacing, with the permeability varying Z/λ times under each pair of poles and generating the corresponding tooth harmonics of the permeability. At this point, the air gap permeability can be written as (1) [16]:

$$\Lambda = \Lambda_0 + \sum_{k=1}^{\infty} \Lambda_0 \left(k \frac{Z}{\lambda} \omega t \right) \tag{1}$$

where Λ_0 is the constant component of the air gap permeability, Λ_k is the kth harmonic amplitude of the air gap permeability, Z is the number of stator slots, and λ is the number of magnetic pole pairs, and ω is the electrical angular velocity.

The magnetic potential at the surface of the permanent magnet during no-load operation of the motor can be expressed as (2) [16]:

$$F = F_m \cos\left(\lambda \zeta\right) \tag{2}$$

where F_m is the magnetic potential amplitude, $\lambda\zeta$ is the spatial angle of the magnetic potential of the permanent magnet concerning the reference axis.

At this point, the air-gap magnetic density at any instant is written as (3):

$$B(\theta,t)=F(\theta,t)\cdot\Lambda(\theta,t)=F_m\cos(\lambda\zeta)\left[\Lambda=\Lambda_0+\sum_{k=1}^{\infty}\Lambda_0\left(k\frac{Z}{\lambda}\omega t\right)\right] \tag{3}$$

From (3), it can be seen that the number of harmonics of the magnetically guided teeth caused by slotting in the air-gap magnetic density waveform is the $kZ/\lambda\pm1$ th harmonic.

2.1.2. Generation of Space Harmonics

Spatial harmonic magnetomotive force is caused by non-uniform distribution of stator windings. It is divided into phase band harmonic magnetomotive force and tooth harmonic magnetomotive force. In this case, the phase-band harmonic component is since the conductor currents distributed along the periphery of the armature do not belong to the same phase of the winding, *i.e.* the transition between phases is not smooth enough and there are jumps; the tooth harmonic component is since the conductors are all concentrated in a finite number of slots and are not uniformly distributed along the armature, resulting in insufficient smoothing of the magnetic potential from slot to slot and jumps, as shown in **Figure 2**.

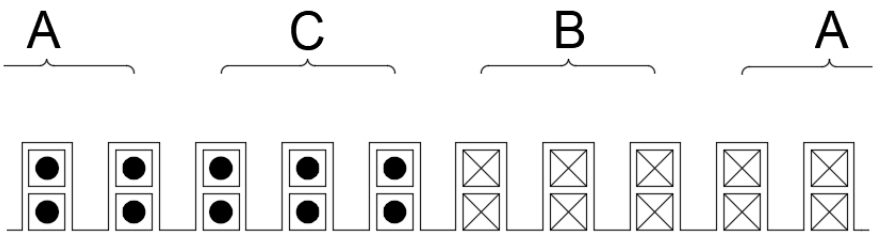

Figure 2. Distribution of phase band windings.

When the stator winding is energized with a three-phase sinusoidal current, the vth harmonic magnetic potentials generated by the A, B, and C phase windings are added together to obtain the vth harmonic synthesized magnetic potentials of the three-phase windings as follows [16]:

$$\begin{aligned} f_v(x,t)&=f_{Av}(x,t)+f_{Bv}(x,t)+f_{Cv}(x,t)\\ &=F_{\phi v}\left[\cos\frac{v\pi}{\tau}x\cos\omega t+\cos v\left(\frac{\pi}{\tau}x-120^\circ\right)\cos(\omega t-120^\circ)\right.\\ &\left.+\cos v\left(\frac{\pi}{\tau}x+120^\circ\right)\cos(\omega t+120^\circ)\right] \end{aligned} \tag{4}$$

where f_{Av}, f_{Bv}, and f_{Cv} are the vth harmonic magnetic potentials of phases A, B, and C, respectively, x is the spatial distance coordinates, and $F_{\phi v}$ is the vth harmonic synthesized magnetomotive force amplitude, and τ is the polar distance.

It has the following pattern:

1) When $v = 3k$, $f_v(x,t) = 0$, so there is no 3rd and multiples of 3rd harmonic.

2) When $v = 6k \pm 1$, $f_v(x,t) = 1.5F_{\phi v}\cos(v\pi x/\tau \pm \omega t)$.

3) When $v = kZ/\lambda \pm 1$, there are magnetomotive force tooth harmonics of the same order as the permeability tooth harmonics.

From Equation (4), the amplitude of the harmonic magnetic potential varies with time and space, while the air gap permeability varies synchronously, and the product of the two is the flux ϕ. There are two types of flux variations, one of which is generated by time-varying currents, *i.e.* the flux is a function of time *t*, and the other is generated by the relative motion between the permanent magnet and the magnetic field, *i.e.* the flux is a function of position variable *x*.

From the law of electromagnetic induction [16]:

$$e = -\frac{\mathrm{d}\psi}{\mathrm{d}t} = -\frac{\mathrm{d}\Phi}{\mathrm{d}t} \tag{5}$$

where e is the induced electromotive force in the loop, ψ is the magnetic chain of the crosslinked loop, and Φ is the loop area flux.

From Equation (5), the change of harmonic magnetic potential will produce induced electromotive force on the surface of the conductor of the stator and rotor, and due to the different flux densities or magnetic field variation strengths in each part of the conductor, resulting in different induced electromotive forces in each part, which in turn form harmonic currents of different sizes inside the conductor and consume in the conductor's internal resistance to form eddy current losses, as shown in **Figure 3**.

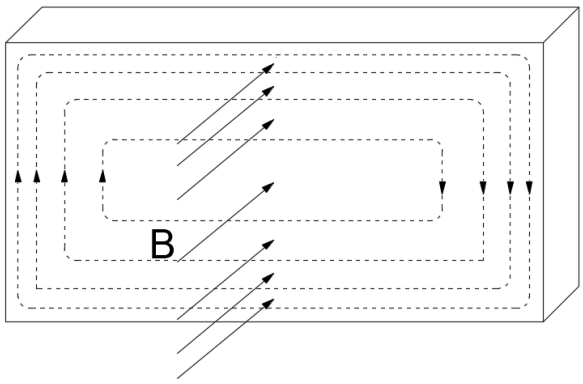

Figure 3. Eddy current path.

2.2. Permanent Magnet Eddy Current Loss Calculation Model

Air gap harmonics (magnetic conductivity harmonics and space harmonics, etc.) generate eddy current losses in the permanent magnets on the surface of the rotor of a surface-mounted permanent magnet synchronous motor. During rotation, the air gap density and the magnetic density of the permanent magnets change accordingly, and the changing density induces eddy currents in the permanent magnets.

The variation of the air-gap flux density at a slot distance can be written in the form of a Fourier series in terms of $\alpha \in [0, 2\pi/Z]$, which is obtained when the slot is in the middle position [17]:

$$B_\delta(\alpha) = B_{av}\left[1 - \sum_{k=1}^{\infty}(-1)^k \beta k_c \alpha_{1k} \cos(kZ\alpha)\right] \tag{6}$$

where

$$\alpha_{1k} = \frac{2\sin\left(k\pi\dfrac{b_1'}{\tau_u}\right)}{k\pi\left[1-\left(k\dfrac{b_1'}{\tau_u}\right)^2\right]},\quad b_1' = \gamma\frac{\delta}{\beta},\quad \gamma = \frac{\left(\dfrac{b_1}{\delta}\right)^2}{5+\dfrac{b_1}{\delta}}$$

$$\beta = \frac{B_{\max}-B_{\min}}{2B_{\max}} = \frac{1+u^2-2u}{2\left(1+u^2\right)},\quad \frac{B_{\min}}{B_{\max}} = \frac{2u}{1+u^2},\quad u = \frac{b_1}{2\delta} + \sqrt{1+\left(\frac{b_1}{2\delta}\right)^2}$$

where B_{av} is the average flux density; τ_u is the slot spacing; u is the voltage specification; b_1' is the total width of the region; and δ is the air gap length, using the equivalent air gap length δ_e proposed by Carter.

From the above equation, it can be seen that the ratio of notch width to air gap length affects the change of air gap flux, *i.e.* keeping the notch width constant, the air gap flux can be reduced by increasing the air gap length, and chipping the permanent magnets can change the length of the equivalent air gap.

Based on the above principle, this paper proposes to cut the corners of the permanent magnets to increase the equivalent air gap length by changing the structural shape of the permanent magnets to reduce the eddy current loss. The tile-type permanent magnet pole chipping scheme is shown in **Figure 4**, where the structural shape of the permanent magnet with right angles at both ends as shown in (a) is changed to a chipped structural shape with angles at both ends of the permanent magnet as shown in (b) without reducing the volume of the permanent magnet.

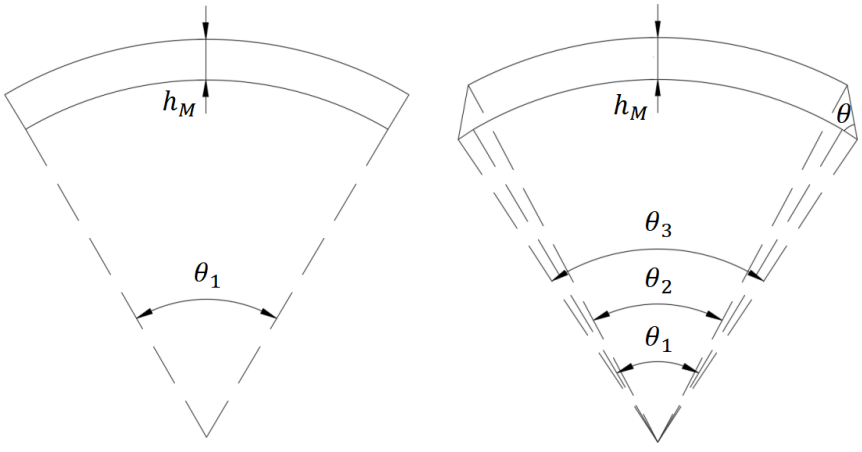

(a) Unchamfered permanent magnet shape (b) Chamfered permanent magnet shape

Figure 4. Unchamfered and chamfered permanent magnet shape.

After chipping, the air gap length in Equation (6) changes and the surface of the permanent magnet poles is no longer isotropic and A is corrected to [18]:

$$K_\alpha = 1 - 1/2\left(1 - h_{M1}/h_M\right)\left(1 - \theta_3/\theta_2\right) \tag{7}$$

According to the clipping angle scheme in this paper, where h_{M1} is taken as 0 in Equation (7).

Substituting K_α into the equivalent air gap length equation, the equivalent air gap after clipping the angle poles is obtained as:

$$\delta_e = K_{st} K_\delta \delta / K_\alpha \tag{8}$$

Because the magnetic permeability of permanent magnets and air permeability is close, it can be considered that the change rule of the magnetic density of permanent magnets and air gap magnetic density change rule is basically the same, and the introduction of the skin effect penetration depth δ_{PM} to consider the influence of the permanent magnet vortex reaction, can be calculated that the air gap harmonics in the permanent magnet internal sensing of the vortex density J_M is [6]:

$$J_m = \sigma \frac{\partial B_\delta(\alpha)}{\partial_t} \mathrm{e}^{-Z/\delta_{PM}} \tag{9}$$

where the rate of attenuation of the magnetic field in the conductor is expressed in terms of the depth of penetration [19]:

$$\delta_{PM} = \frac{1}{\sqrt{\pi f \sigma \mu}} \tag{10}$$

where δ_{PM} is the harmonic penetration depth in the permanent magnet, μ is the magnetic permeability of the material, σ is the conductivity of the material, and f is the harmonic frequency.

According to the Poincarin vector [20], the power penetrating the closed surface S from within the volume V is:

$$P = \oint_S (\mathbf{E} \times \mathbf{H}) \mathrm{d}S = \int_V \nabla \cdot (\mathbf{E} \times \mathbf{H}) \mathrm{d}V \tag{11}$$

where $\mathbf{E}$ is the electric field strength, $\mathbf{J}$ is the eddy current density, $\mathbf{H}$ is the magnetic field strength.

Since the permanent magnet hysteresis loss exists only under special conditions, the permanent magnet loss is almost exclusively eddy current loss, so the formula for calculating the permanent magnet eddy current loss can be simplified as [21]:

$$P = \int_V \mathbf{E} \cdot \mathbf{J} \mathrm{d}V = \int_V \frac{\mathbf{J}^2}{\sigma} \mathrm{d}V = \int_V \rho \mathbf{J}^2 \mathrm{d}V \tag{12}$$

where V is the volume of the PM, ρ is the permanent magnet resistivity.

According to the integral form of Faraday's law of electromagnetic induction, we get:

$$\oint_l \mathbf{E} \mathrm{d}l = -\frac{\mathrm{d}\phi}{\mathrm{d}t} = -\frac{\mathrm{d}}{\mathrm{d}t} \iint_S \mathbf{B} \mathrm{d}S \tag{13}$$

where ϕ is the total magnetic flux in the eddy current path, S is the total area in the vortex path.

Substituting $\mathbf{E} = \rho\mathbf{J}$ into the above equation gives:

$$\oint_l \mathbf{J}\mathrm{d}l = \frac{1}{\rho}\oint_l \mathbf{E}\mathrm{d}l = -\frac{1}{\rho}\frac{\mathrm{d}}{\mathrm{d}t}\iint_S \mathbf{B}\mathrm{d}S \tag{14}$$

From Equations (6)-(12), it can be seen that the clipping angle can increase the equivalent air gap length to reduce the harmonic flux rate of change, and the eddy current density decreases with the decrease of the flux rate of change, so that the eddy current loss becomes smaller. Then, from Equation (12) and Equation (14), it can be seen that the permanent magnet eddy current loss is determined by the permanent magnet resistivity and eddy current density, in the case of the permanent magnet resistivity is unchanged, the magnetic flux density on the permanent magnet can reflect the size of the eddy current density.

3. Finite Element Simulation of Eddy Current Loss in Permanent Magnets

3.1. Electromagnetic Field Finite Element Simulation Model

In this paper, a 25 kW table-applied permanent magnet synchronous motor is taken as an example, it has no metal sheath on the surface of the permanent magnet and is made of carbon fiber tied, and its detailed parameters are shown in Table 1. According to the parameters of Table 1, the finite element simulation two-dimensional model of the surface-mounted permanent magnet synchronous motor is drawn, as shown in Figure 5. Finite element calculation mesh using triangular mesh, taking into account the main study in this paper the eddy current loss of permanent magnets, so the permanent magnets, and permanent magnets near the carbon fiber protective sleeve and air gap in the mesh partition to do encrypted processing, set up the triangular mesh length of not more than 0.4 mm, the permanent magnets a little far away from the windings part of the mesh set up the mesh length of not more than 0.5 mm, far away from the permanent magnets of the stator and rotor part of the mesh set up the mesh length of not more than 5 mm. The mesh length is not more than 5 mm, and the meshing results are shown in Figure 6.

Table 1. Parameters of surface-mounted permanent magnet synchronous moto.

Parameters	Numerical values
Rated power/KW	25
Rated speed/(r/min)	63,000
Pair series	4
Frequency/HZ	2100
Stator outside diameter/mm	130
Stator bore/mm	85
Rotor outside diameter/mm	72.2
Thickness of permanent magnet/mm	4

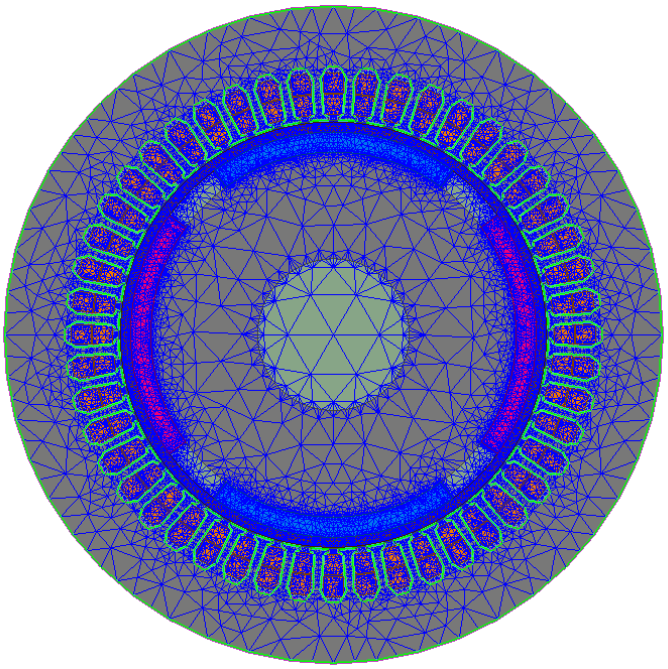

Figure 5. 2D model diagram of permanent magnet synchronous motor.

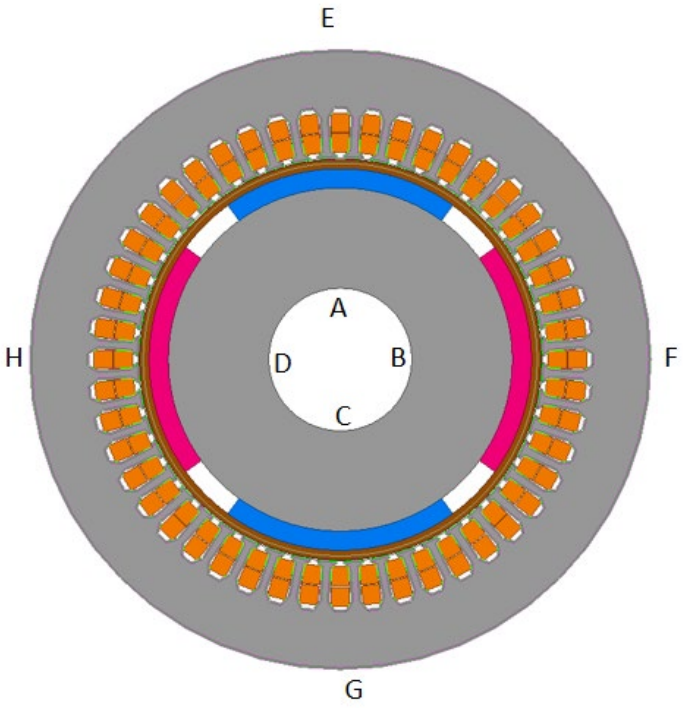

Figure 6. Grid section of permanent magnet synchronous motor.

3.2. Two-Dimensional Time-Stepping Finite Element Simulation of Permanent Magnet Synchronous Motor

To simplify the analysis, the following assumptions are made:

1) Neglecting the end effect of the eddy current, only the axial component of the

rotor eddy current is considered.

2) The material is isotropic and the hysteresis effect of the ferromagnetic material is neglected.

3) Neglect the temperature effects of the magnetic permeability μ and the electric conductivity σ, which are only spatial functions.

4) Negligible eddy currents in the stator-rotor laminated core and current source current region.

Describing the field in terms of the magnetic field vector magnetic potential A, the problem of the fixed solution of the transient electromagnetic field can be expressed as [20]:

$$\begin{cases} \dfrac{\partial}{\partial x}\left(\nu\dfrac{\partial A}{\partial x}\right)+\dfrac{\partial}{\partial y}\left(\nu\dfrac{\partial A}{\partial y}\right)=-\left(J_Z-\sigma\dfrac{\mathrm{d}A}{\mathrm{d}t}\right) \\ \nu\dfrac{\partial A}{\partial n}\Big|_{l^-}-\nu\dfrac{\partial A}{\partial n}\Big|_{l^+}=J_s \\ A|_{ABCD}=A|_{EFGH}=0 \end{cases} \tag{15}$$

where A is the internal magnetic field vector potential of the motor, ν is the magnetoresistivity, J_Z is the source current density, and J_s is the permanent magnet equivalent surface current density, and $\sigma \mathrm{d}A/\mathrm{d}t$ is the eddy current density, and $ABCD$ and $EFGH$ are motor boundaries.

Where the magnetic field vector potential A is given by the following equation [17]:

$$\mathbf{B}=\nabla\times\mathbf{A} \tag{16}$$

From the Coulomb condition, the magnetic field vector potential is defined as follows [17]:

$$\nabla\cdot\mathbf{A}=0 \tag{17}$$

In the two-dimensional case, A has only Z-axis components, in the case of a two-dimensional field containing eddy currents [17]:

$$-\nabla\cdot\left(\frac{1}{\mu}\nabla A_Z\right)+\sigma\frac{\partial A_Z}{\partial t}=0 \tag{18}$$

The following component form is derived from the definition of the flux density vector [17]:

$$Bx=\frac{\partial A_Z}{\partial y},By=-\frac{\partial A_Z}{\partial x} \tag{19}$$

$$B=\sqrt{\left(\frac{\partial A_Z}{\partial x}\right)^2+\left(\frac{\partial A_Z}{\partial y}\right)^2} \tag{20}$$

According to Stokes' theorem, the magnetic flux Φ [17]:

$$\Phi=\int_a B\cdot\mathrm{d}a=\int_a rotA\cdot\mathrm{d}a=\oint_\Gamma A\cdot\mathrm{d}l \tag{21}$$

The equation for the magnetic lines of force in a plane field is [17]:

$$\mathbf{B}\times\mathbf{dl}=\left(\frac{\partial A_Z}{\partial y}\mathbf{i}-\frac{\partial A_Z}{\partial x}\mathbf{j}\right)\times\left(\mathrm{d}x\mathbf{i}+\mathrm{d}y\mathbf{j}\right)=\left(\frac{\partial A_Z}{\partial y}\mathrm{d}y+\frac{\partial A_Z}{\partial x}\mathrm{d}x\right)\mathbf{k}=0 \tag{22}$$

The full differential of the isovector A line is [17]:

$$\mathrm{d}A = \frac{\partial A_Z}{\partial x}\mathrm{d}x + \frac{\partial A_Z}{\partial y}\mathrm{d}y = 0 \tag{23}$$

So, the magnetic lines of force are then isovectorial A lines.

In this paper, no-load and load simulations of permanent magnet synchronous motors are carried out. Figures 7-10 show the magnetic induction intensity cloud diagram and magnetic force line cloud diagram of the permanent magnet synchronous motor at no load and load, respectively. According to the simulation cloud diagrams, the magnetic lines of force and magnetic induction intensity of the prototype are symmetric along the center of the magnetic poles and are uniformly distributed at no load, but at load the magnetic field is distorted due to the armature reaction, resulting in that the magnetic lines of force and magnetic induction intensity are no longer uniformly distributed. In the no-load state, because of zero current in the winding, does not produce three-phase winding magnetic potential, so there is only the magnetic conduction harmonics due to slotting in the motor; in the load state, the winding is a non-zero three-phase sinusoidal current, not only the magnetic induction intensity of the permanent magnets is increased compared to the no-load state, but there are more magnetic potential harmonics due to three-phase winding in the motor. Whether in the no-load state or load state, the magnetic induction intensity and the size of the magnetic lines of force at both ends of each permanent magnet are maximum, according to Equation (5), the induced electromotive force generated on both sides of the permanent magnet is the maximum, which produces the most eddy current losses.

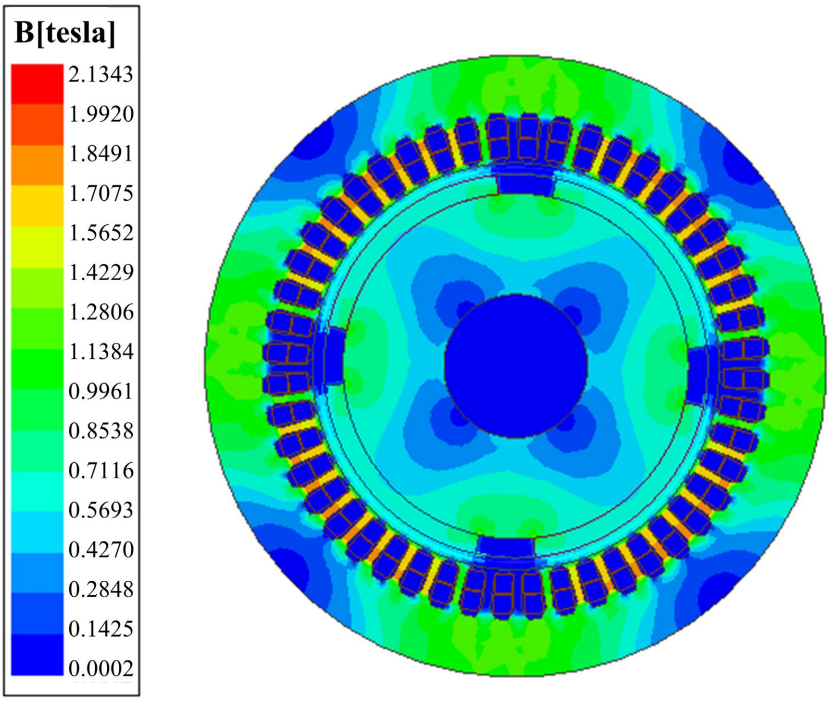

Figure 7. Unloaded magnetic induction intensity cloud.

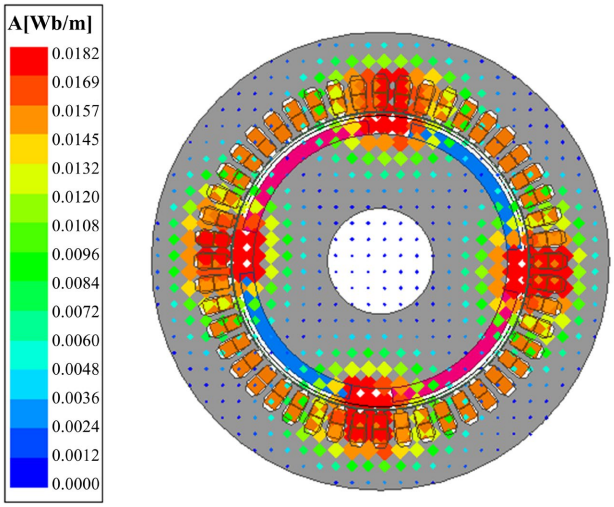

Figure 8. Cloud of unloaded magnetic lines.

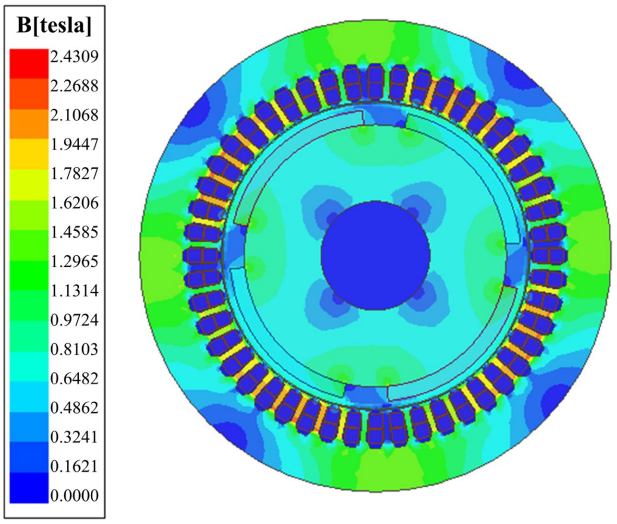

Figure 9. Load magnetic induction intensity cloud.

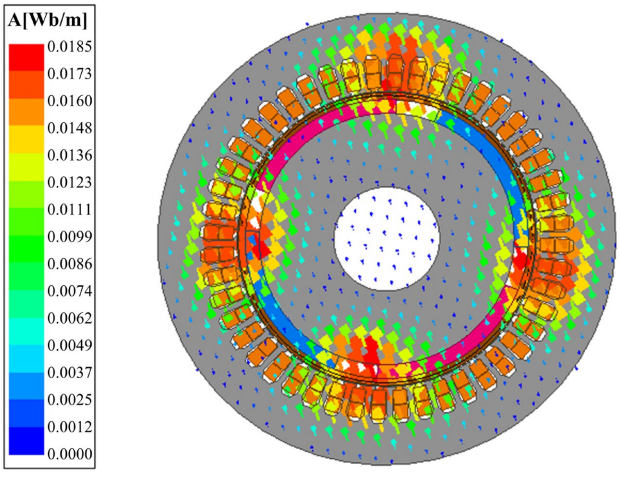

Figure 10. Load magnetic line cloud.

Since it is the various harmonics that lead to the generation of eddy current losses in the permanent magnets, and the air-gap radial magnetization waveform contains the various harmonics, the air-gap radial magnetization waveform of the motor under the rated load is extracted as shown in Figure 11. It can be seen that the prototype air gap radial magnetization jumps up and down, and the sine wave tends to flatten. This is due to the cogging effect, which makes the air gap magnetomagnetism drop significantly at the position of the slot.

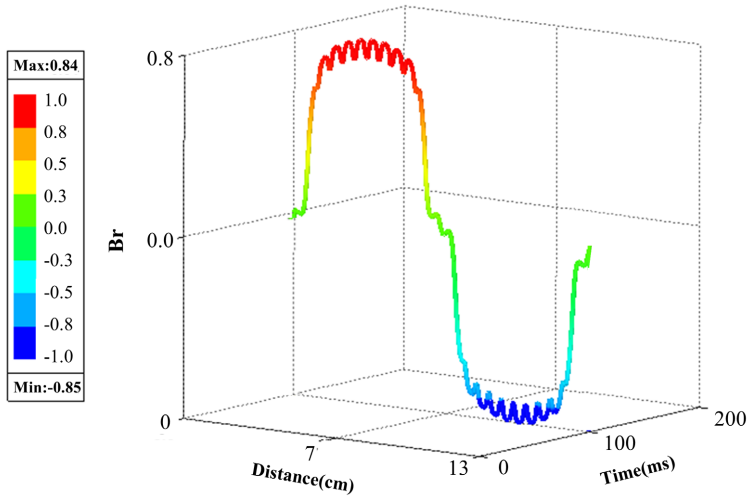

Figure 11. Radial magnetic density of air gap.

The use of Fourier analysis of the motor air gap radial magnetic field decomposition can be obtained 1, 3, 5, 7, and other odd-order harmonic components, there are no even-order harmonic components because the magnetic field waveform is symmetrical concerning the centerline of the magnetic poles. Figure 12 shows the magnitude of the magnetic induction of each odd-order harmonic component after Fourier decomposition, and it can be seen that in addition to the space harmonics (phase band harmonics) and the notch harmonics, there are also the 3rd, 9th, 15th and 21st harmonics, which are saturated harmonics due to the material properties.

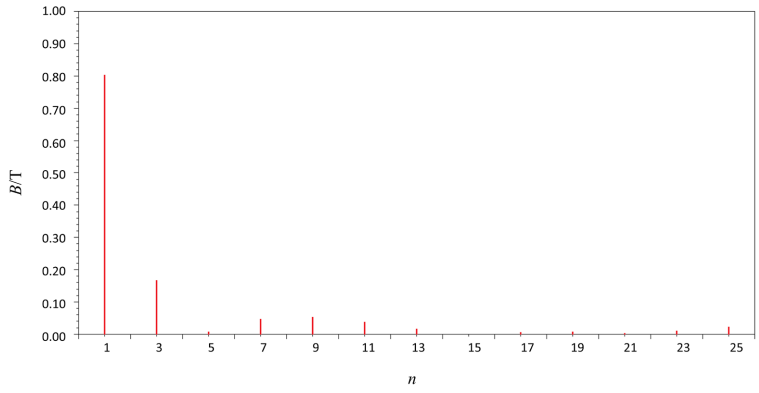

Figure 12. Harmonic components of the radial magnetization of the air gap.

According to the flute law, the eddy currents in the permanent magnet in turn generate an induced magnetic field that impedes the variation of this harmonic field, and this induced magnetic field causes the high-frequency harmonic field to decay in the axial direction of the permanent magnet. The farther the permanent magnet is from the air gap, the smaller the eddy current loss inside the permanent magnet.

The frequency of the vth harmonic is a multiple of the fundamental frequency, and as the number of harmonics rises, the depth of skin penetration decreases, resulting in higher current densities in the rotor sheath as well as on the permanent magnets.

When the prototype is operated at rated condition, $\delta_9 = 4.27$ mm, $\delta_{11} = 3.86$ mm, it can be seen that the high harmonic penetration depth of 11 and above is less than the thickness of the permanent magnet, and the skin effect can not be ignored, so it is necessary to set up an encrypted mesh of the skin layer of the permanent magnet during the simulation of the permanent magnet's eddy current loss.

3.3. Effect of PM Chipping Angle θ on PM Eddy Current Loss

For this paper chipping program, the chipping angle θ is calculated to know that the chipping angle θ is less than 25˚ when the motor permanent magnets will be intersected together, so the minimum value of the chipping angle θ is set to 30˚. θ angle in addition to the initial 90˚, the other selected angle is equal to 60˚, 45˚, and 30˚, to study the influence of the chipping angle of the permanent magnets for permanent magnet eddy current loss.

Based on the selected motor parameters and set boundary conditions in this paper, the magnetic line cloud diagrams of permanent magnets with four cutting angles are obtained by finite simulation as shown in **Figure 13**, where the magnitude of the magnetic lines represents the magnetic induction intensity per unit area. As can be seen from the magnetic line cloud diagram in **Figure 13**, the maximum value of the magnetic lines of force appears at both sides of the permanent magnet, that is, the place where the permanent magnet is clipped, and the maximum value of the permanent magnet's magnetic lines of force decreases gradually with the decrease of the clipping angle θ, decreasing from 0.0185 Wb/m at $\theta = 90^\circ$ to 0.0178 Wb/m at $\theta = 30^\circ$. According to Equation (14), it can be seen that the eddy current density and the size of the magnetic induction strength are proportional to the relationship, that is, the eddy current loss and the size of the magnetic lines of force are also proportional to the relationship, so the permanent magnets for the chipping process can reduce its eddy current loss, and the smaller the permanent magnet chipping eddy current loss will be less.

The values of average flux density and eddy current loss of permanent magnet with different clipping angles θ extracted from the simulation results are shown in **Table 2**, from which it can be seen that as the clipping angle θ decreases, the average flux density and eddy current loss of the permanent magnet is gradually

reduced. The permanent magnet eddy current loss decreases from 15.81 W for $\theta = 90^{\circ}$ to 14.26 W for $\theta = 30^{\circ}$, which is a reduction of 9.8%. The size of the permanent magnet flux density not only affects the size of the eddy current loss but also affects the performance of the motor, according to the simulation results, the permanent magnet chipping angle $\theta = 30^{\circ}$ motor torque is only 0.51% lower than that of the unchipped angle ($\theta = 90^{\circ}$), which has a negligible effect on the performance of the motor. Therefore, the simulation results show that the eddy current loss of permanent magnets can be significantly reduced by chipping the end face of permanent magnets to change its structural shape under the condition of hardly affecting the performance of the motor.

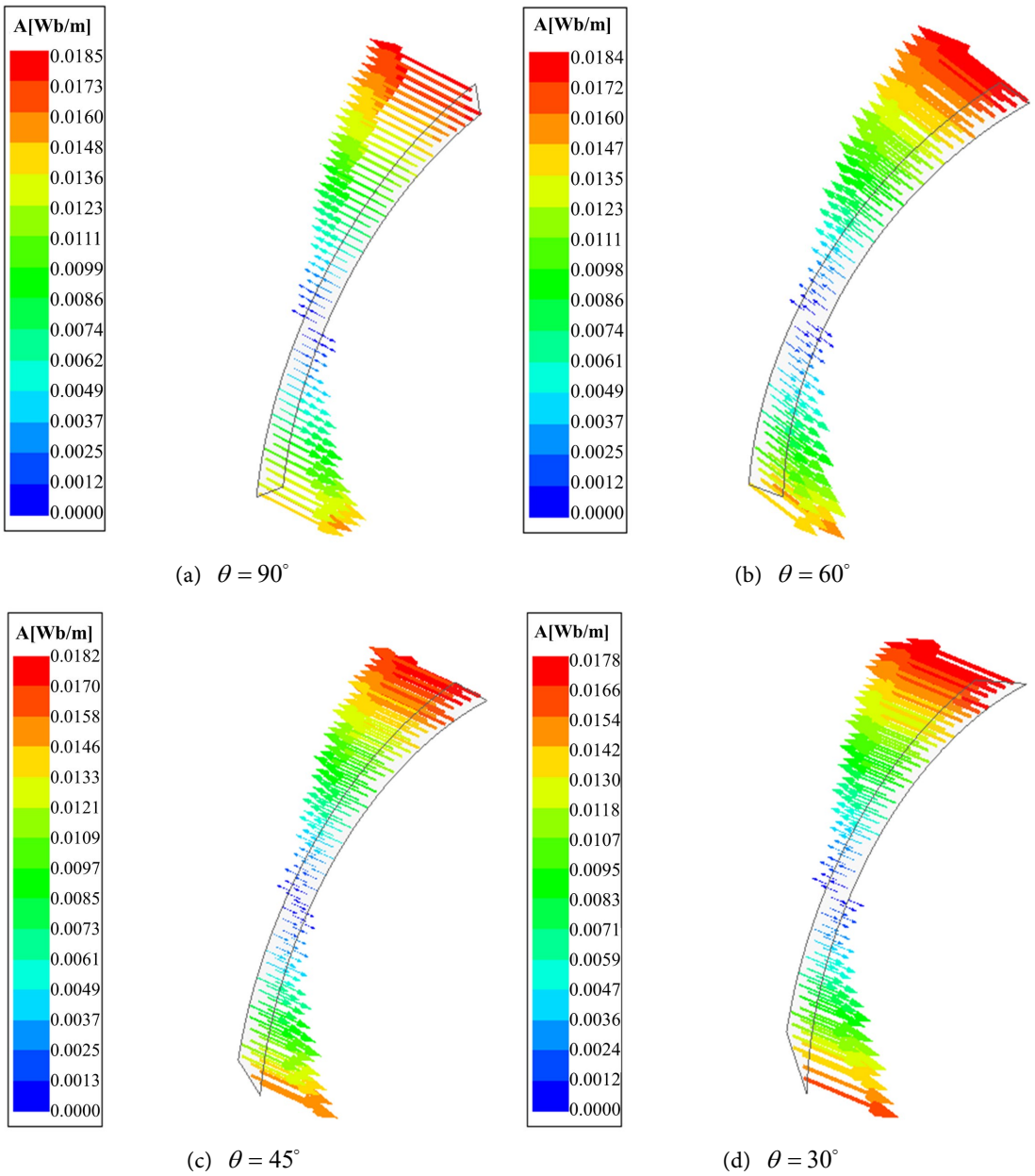

Figure 13. Clouds of magnetic lines of permanent magnets with 4 kinds of cutting angles.

Table 2. Average flux density and eddy current loss values of permanent magnets with different chipping angles θ.

θ/(˚)	Average magnetic flux density/T	PM eddy current loss/W
90	0.71	15.81
60	0.70	15.12
45	0.69	14.80
30	0.67	14.26

4. Simulation Analysis of Permanent Magnet Temperature Field

The permanent magnet eddy current losses are transformed into heat, which is transferred to the surfaces of the motor components by conduction and then emitted to the surrounding cooling medium by convection and radiation. Since heat exchange in the motor is a very complex process, the permanent magnet solution region needs to be simplified for simplicity of calculation.

The following assumptions are made about the solution region and boundary conditions:

1) Neglecting the penetration depth of the skin effect, the heat generated by eddy current losses is assumed to be internally generated.

2) Neglect the effect of the motor stator on the rotor temperature field.

3) Set the permanent magnet eddy current loss to be distributed evenly throughout the block, *i.e.* the eddy current loss of the entire permanent magnet is distributed evenly throughout this permanent magnet.

4) Assuming that the heat dissipation of the permanent magnet is in the form of mixed natural convection.

Basic motor heat transfer equation:

1) Thermal conduction [22]:

$$q = -kgradX \tag{24}$$

where q is the heat flow density, k is the thermal conductivity, $gradX = \partial T/\partial n\left(\mathbf{i}+\mathbf{j}+\mathbf{k}\right)$ is the temperature gradient, $\mathbf{i},\mathbf{j},\mathbf{k}$ are unit vectors of x, y, and z axes.

2) Heat convection [22]:

$$q = h\left(T_S - T_B\right) \tag{25}$$

where h is the convective heat transfer coefficient, T_S is the temperature of the surface of the object, T_B is the temperature of the surrounding medium.

3) Thermal radiation [22]:

$$q = \varepsilon\varsigma\left(T_1^4 - T_2^4\right) \tag{26}$$

where ε is a factor whose magnitude varies with the surface condition of the heat generator, $\varsigma = 5.7\times10^{-8}\ \mathrm{W/m^2\cdot K}$ is the Boltzmann constant for a pure blackbody, T_1 is the surface temperature of the heating element, and T_2 is the absolute temperature of the surrounding medium.

In this paper, the motor temperature field is calculated using a more realistic conventional steady state algorithm, according to the relevant theory of heat transfer, the three-dimensional transient heat conduction equation is as follows:

$$\begin{cases} K_x \dfrac{\partial^2 T}{\partial x^2} + K_y \dfrac{\partial^2 T}{\partial y^2} + K_z \dfrac{\partial^2 T}{\partial z^2} + q = c\gamma \dfrac{\partial T}{\kappa} \\ -K \dfrac{\partial T}{\partial n}\Big|_{S_1} = 0 \\ -K \dfrac{\partial T}{\partial n}\Big|_{S_2} = \alpha\left(T - T_e\right) \end{cases} \tag{27}$$

where T is the temperature, q is the density of the heat source, c is the specific heat capacity, and γ is the density, and κ is for time, and S_1, S_2 are the adiabatic boundary surface and the heat dissipation boundary surface, and α is the heat dissipation coefficient of the S_2 surface, and K is the normal thermal conductivity of the S_1 and S_2 surfaces, and K_x, K_y, K_z are the thermal conductivity of the medium in this direction.

In Ansys Icepak, we constructed three-dimensional models of permanent magnets with a thickness of 4 mm without cutting angle ($\theta = 90^\circ$) and with cutting angle $\theta = 30^\circ$, and imported the simulation results of two-dimensional time-stepping finite elements into Ansys Icepak to simulate the steady-state temperature field of the two types of permanent magnet structures.

The simulation settings are as follows:

1) Set the density of NdFeB permanent magnet material to 7700 kg/m^3, specific heat capacity 465 J/kg·K, and thermal conductivity 7 W/m·K.

2) The air path was set up with a mixed natural convection using a flow-solid combination, set up as a turbulence model, given an inlet velocity of 10 m/s and an ambient temperature of 20˚C.

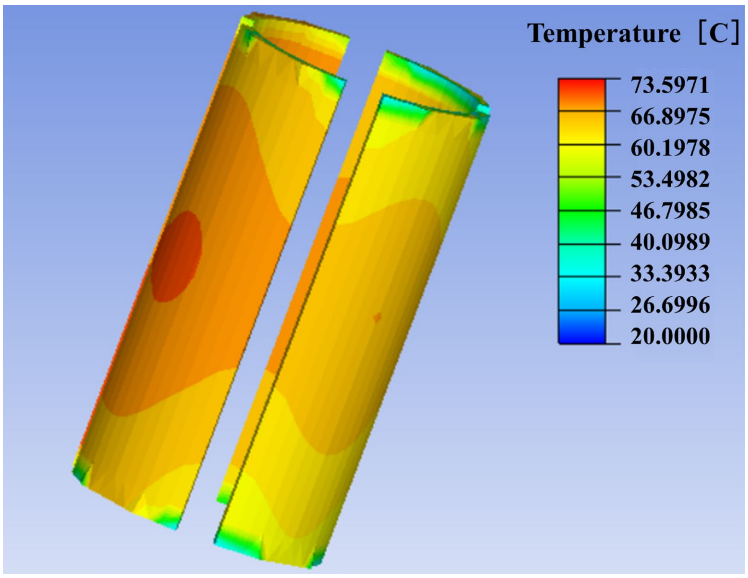

Figure 14. Temperature field of $\theta = 90^\circ$ permanent magnet.

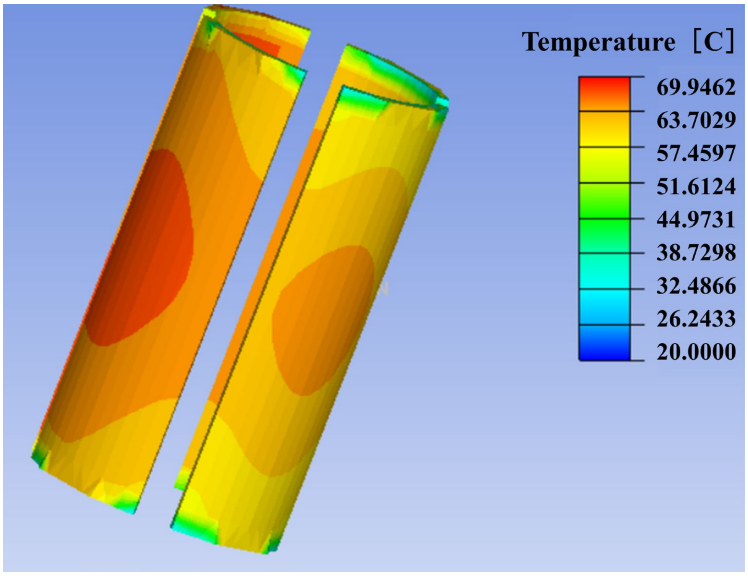

Figure 15. Temperature field of $\theta = 30^{\circ}$ permanent magnet.

After finite element simulation calculations, the temperature field cloud diagrams of the two structures of permanent magnets are obtained, as shown in **Figure 14** and **Figure 15**, from which it can be seen that the highest temperature point of the permanent magnets occurs in the middle part of the permanent magnets instead of the vicinity of the maximum point of the eddy current loss of the permanent magnets, which is due to the simulation assumption that the eddy current loss of the permanent magnets is the whole piece of the average distribution of the permanent magnets caused by the simulation. From **Figure 14** and **Figure 15**, it can also be seen that the maximum temperature of the permanent magnet at $\theta = 90^{\circ}$ and $\theta = 30^{\circ}$ is 73.60˚C and 69.95˚C, respectively, which indicates that the maximum temperature of the permanent magnet can be reduced by about 5% by changing the structure of the permanent magnet to the clipping angle $\theta = 30^{\circ}$, which indirectly proves that the eddy-current loss of the permanent magnet can be reduced by changing the structure of the permanent magnet to the clipping angle form.

5. Conclusions

Aiming at the problem of high temperature and even demagnetization failure of permanent magnet due to permanent magnet eddy current loss in permanent magnet synchronous high-speed motors, which seriously affects the high-speed, stable, and reliable operation of motors, a method is proposed to reduce the eddy current loss of permanent magnets by cutting the angle of permanent magnet poles to change the shape of the permanent magnet structure. This paper adopts theoretical derivation and finite element simulation to take a 25 KW surface-type permanent magnet synchronous high-speed motor as an object, studies the influence of permanent magnet pole shaving angle θ on its eddy current loss and operating temperature, and obtains the following conclusions:

1) The theoretical calculation model of permanent magnet eddy current loss of permanent magnet synchronous high-speed motor is deduced, and it is theoretically proved that the permanent magnet eddy current loss can be reduced by chipping the magnetic poles of the permanent magnet to change its structural shape.

2) The permanent magnet eddy current loss of permanent magnet synchronous high-speed motor decreases with the decrease of pole clipping angle A. This is because as the clipping angle decreases, the air gap magnetization waveform improves, thus reducing the generation of harmonic magnetization. Under the condition of almost not affecting the performance of the motor, the eddy current loss of permanent magnet pole clipping angle θ of 30˚ can be reduced by 9.8% compared with the unclipped angle.

3) The use of permanent magnet pole chipping structure can reduce the permanent magnet synchronous high-speed motor permanent magnet operating temperature, in the rated power of permanent magnet pole chipping for the maximum temperature, the unchipped can be reduced by about 5%.

Acknowledgements

The above study was supported by the National Natural Science Foundation of China (51875198), Key Project of Hunan Provincial Department of Education: Research on the Formation and Evolution Mechanism of Oil Film Holes in Hydrostatic Motorized Spindle and Its Active Control Method (23A0360) and the Xiangtan Science and Technology Bureau Science and Technology Research Project "Research on Active Control and Evaluation Technology of Variable Mass Unbalanced Rotor System of Ultra-High Speed Maglev Permanent Magnet Synchronous Motorized Spindle" (GX-YB20221004).

Conflicts of Interest

The authors declare no conflicts of interest regarding the publication of this paper.

References

[1] Xiong, W.L., Sun, W.B., Liu, K. and Xu, M.H. (2021) Active Magnetic Bearing Technology Development in High-Speed Motorized Spindles. *Journal of Mechanical Engineering*, **57**, 1-17.

[2] Zhao, X.H., Deng, Z.Q., Wang, X.L. and Mei, L. (2009) Research Status and Development of Permanent Magnet Biased Magnetic Bearings. *Transactions of China Electro-Technical Society*, **24**, 9-20.

[3] Zhu, H.Q. and Ju, J.T. (2014) Development of Three-Pole Magnetic Bearings and Key Technologies. *Proceedings of the CSEE*, **34**, 1360-1367.

[4] Tong, W.M., Li, J.S., Cao, B.Y. and Wu, S.G. (2021) Three-Dimensional Analytical Model of Eddy Current Loss of Permanent Magnet in High Frequency Axial Flux Permanent Magnet Machine. *Proceedings of the CSEE*, **41**, 1992-2002.

[5] Zhu, Z.Q., Ng, K., Schofield, N. and Howe, D. (2004) Improved Analytical Modelling of Rotor Eddy Current Loss in Brushless Machines Equipped with Surface-Mounted Permanent Magnets. *IEE Proceedings—Electric Power Applications*, **151**, 641-650. https://doi.org/10.1049/ip-epa:20040546

[6] Tang, R.Y., Chen, P., Tong, W.M. and Han, X.Y. (2015) Analytical Calculation of Eddy Current Loss Accounting for Eddy Current Reaction. *Transactions of China Electrotechnical Society*, **30**, 1-10.

[7] Gao, P.F., Fang, J.C., Han, B.C. and Sun, J.J. (2013) Analysis of Rotor Eddy-Current Loss in High-Speed Permanent Magnet Motors. *Micromotors*, **46**, 5-11.

[8] Dong, C.Y., Li, Y., Ding, S.Y. and Deng, Y.Q. (2015) Iron Loss Analysis of Switched Reluctance Motor. *Electric Machines and Control*, **19**, 58-65.

[9] Stone, D.A., Mellor, P.H., Howe, D. and Atallah, K. (2000) Rotor Loss in Permanent-Magnet Brushless AC Machines. *IEEE Transactions on Industry Applications*, **36**, 1612-1618. https://doi.org/10.1109/28.887213

[10] Toda, H., Xia, Z., Wang, J., Atallah, K. and Howe, D. (2004) Rotor Eddy-Current Loss in Permanent Magnet Brushless Machines. *IEEE Transactions on Magnetics*, **40**, 2104-2106. https://doi.org/10.1109/tmag.2004.832481

[11] Polinder, H. and Hoeijmakers, M.J. (1999) Eddy-Current Losses in the Segmented Surface-Mounted Magnets of a PM Machine. *IEE Proceedings—Electric Power Applications*, **146**, 261-266.

[12] Zhou, F.Z. (2008) Investigation of Rotor Eddy-Current Loss in High-Speed PM BLDC Motors. Ph.D. Dissertation, Zhejiang University.

[13] Dajaku, G. and Gerling, D. (2011) Eddy Current Loss Minimization in Rotor Magnets of PM Machines Using High-Efficiency 12-Teeth/10-Slots Winding Topology. 2011 *International Conference on Electrical Machines and Systems*, Beijing, 20-23 August 2011, 1-6. https://doi.org/10.1109/icems.2011.6073360

[14] Dajaku, G., Xie, W. and Gerling, D. (2014) Reduction of Low Space Harmonics for the Fractional Slot Concentrated Windings Using a Novel Stator Design. *IEEE Transactions on Magnetics*, **50**, 1-12. https://doi.org/10.1109/tmag.2013.2294754

[15] Tian, Z.Y., Zhu, C.S. and Wang, D. (2011) Rotor Eddy Current Loss in High-Speed Permanent Magnet Motors for Flywheel Energy Storage System. *Journal of Zhejiang University* (*Engineering Science*), **45**, 451-457.

[16] Ge, B.J., Liang, Y.P. and Wen, J.B. (2016) Ch. 10. Magnetic Potential of the AC Winding. In: *Electric Machinery*, 3rd Edition, China Electric Power Press, 104-113.

[17] Chai, F., Fei, Y.L. and Yu, Y.J. (2018) Ch. 7. Characteristics of Rotating Motors. In: *Rotary Motor Design China*, China Machine Press, 352-358.

[18] Ou, J.F., Shen, X.F. and Yu, W.H. (2020) Electromagnetic Design and Loss Analysis of High-Power and High-Speed Permanent Magnet Motor. *Electric Machines & Control Application*, **47**, 46-51.

[19] Tang, R.Y. (2015) Ch. 5. The Main Coefficient in the Calculation of Magnetic Circuit of Permanent Magnet Motor. In: *Modern Permanent Magnet Machines—Theory and Design China*, China Machine Press, 113-123.

[20] Dong, J.N., Huang, Y.K., Jin, L. and Lin, H.Y. (2014) Review on High Speed Permanent Magnet Machines Including Design and Analysis Technologies. *Proceedings of the CSEE*, **34**, 4640-4653.

[21] Chen, P., Tang, R.Y., Tong, W.M. and Jia, J.G. (2015) Permanent Magnet Eddy Current Loss and Its Influence of High Power Density Permanent Magnet Synchronous Motor. *Transactions of China Electrotechnical Society*, **30**, 1-9.

[22] Chen, S.K. (2000) Ch. 7. Calculation of Heat Generation. In: *Motor Design China*, China Machine Press, 121-127.